New Derivatives of Farnesylthiosalicylic Acid (Salirasib) for Cancer Treatment: Farnesylthiosalicylamide Inhibits Tumor Growth in Nude Mice Models

Liat Goldberg,[†] Roni Haklai,[†] Victor Bauer,[‡] Aaron Heiss,[§] and Yoel Kloog*,[†]

Department of Neurobiology, The George S. Wise Faculty of Life Sciences, Tel-Aviv University, Tel Aviv, Israel, Concordia Pharmaceuticals, Inc., 1550 Sawgrass Corporate Parkway, Sunrise, Florida, Ricerca Biosciences, 7528 Auburn Road, Concord, Ohio

Received April 23, 2008

The Ras inhibitor *S-trans,trans*-farnesylthiosalicylic acid (FTS, Salirasib) interferes with Ras membrane interactions that are crucial for Ras-dependent transformation. It remains unknown whether modifications of the carboxyl group of FTS can affect its activity. Here we show that specific modifications of the FTS carboxyl group by esterification or amidation yield compounds with improved growth inhibitory activity, compared to FTS, as shown in Panc-1 and U87 cells. The most potent compounds were FTS-methoxymethyl ester and FTS-amide. However, selectivity toward active Ras-GTP, as known for FTS, was apparent with the amide derivatives of FTS. FTS-amide exhibited the overall highest efficacy in inhibition of Ras-GTP and cell growth. This new compound significantly inhibited growth of both Panc-1 tumors and U87 brain tumors. Thus amide derivatives of the FTS carboxyl group provide potent cell-growth inhibitors without loss of selectivity toward the active Ras protein and may serve as new candidates in cancer therapy.

Introduction

Ras proteins act as key regulators of cell signaling pathways. Their activation is dependent upon binding to a GTP[a] nucleotide[1−3] and association to the plasma membrane.[4−9] Active Ras proteins trigger an array of cellular messengers transducing key signals regulating proliferation,[2] migration,[10−12] and cell death.[13] Termination of these signals involves hydrolysis of the Ras bound GTP to GDP.[14] Several mutated forms of Ras are defective in their GTP hydrolysis liability and are therefore constitutively active.[1,3] These oncogenic Ras proteins, which are found in many cancer types, contribute to malignancy and are therefore considered favored targets for directed therapy.[15]

Association of Ras to the plasma membrane has been shown to be crucial for its activity in both the wild type and the mutated constitutively active forms.[2,16,17] At least two structural elements are required for this association; the first is a farnesylcysteine carboxy methyl ester at the carboxy terminal of Ras, and the other element resides at the adjacent upstream sequence and varies among different Ras isoforms.[5,6] Normal Ras activity requires specifically the farnesyl isoprenoid moiety,[16,18] which acts as a specific recognition unit to allow binding of H-Ras with galectin-1[19,20] and K-Ras with galectin-3,[21] promoting strong membrane association and robust signaling. These galectins possess a hydrophobic binding pocket, the putative farnesyl binding site.[20] Galectin-1 was shown to drive H-Ras-GTP nanocluster formation and to be an integral component of the H-Ras-GTP nanocluster, a site at which Raf is activated.[22] Together, these findings mark the farnesyl-binding pockets as outstanding targets for Ras directed therapy, assuming that compounds that would block such sites will act as Ras inhibitors.

A strong affirmation to this concept came with the design of the specific Ras inhibitor, S-*trans-trans*-farnesylthiosalicylic acid (Salirasib). FTS was designed to mimic the farnesyl moiety in the carboxy terminal of Ras[23] and was found to induce accelerated dislodgement of Ras from the cell membrane and subsequent degradation of the protein.[24] FTS was also found to be highly efficient in inhibiting growth of many types of cancer cell lines both in vitro and in vivo as well as inhibiting migration of several glioblastoma cell lines.[10,25−29] Biochemical and gene expression profiling experiments provided strong support to the notion that the growth inhibitory effects of FTS are the result of inhibition of Ras-dependent signaling involved in tumor progression and maintenance.[26,30,31]

In previous work, efforts were made to find new FTS derivatives that might improve the anticancer effect of the drug. These compounds were all based on the FTS backbone and were modified on different positions such as the benzene ring or different lengths of the isoprenoid chain. These studies established that the minimal length of the isoprenoid group required for the inhibition of Ras is C15 (farnesyl) because the C10 isoprenoid derivative geranylthiosalicylic acid was inactive.[23,32] Although some of the previously described compounds, including 5-F-FTS and 5-Cl-FTS, were found to be effective inhibitors of cell growth in Ras transformed cells, none proved to be superior to FTS.[32] It remains unknown whether modifications of the carboxyl group of FTS could have an impact on its anti Ras activity. This prompted us to search for new compounds that may improve FTS's potency in various cancer types and perhaps shed some more light on Ras−membrane interactions. In the present study, we investigated the efficacy of several new FTS derivatives with modifications to their carboxyl group. During the design of these compounds, an important consideration taken into account was the degree of applicability in a brain tumor model. In a previous work, FTS was shown to penetrate the BBB in very low concentrations, possibly due to its free carboxyl end.[33] Therefore, the new compounds described here were designed to allow possible better penetration by means of various modifications that increase the lipophilicity of the molecule. The potency of the new derivatives was examined in

* To whom correspondence should be addressed. Phone: 972-3-640-9699. Fax: 972-3-640-7643. E-mail: kloog@post.tau.ac.il.

[†] Department of Neurobiology, The George S. Wise Faculty of Life Sciences.

[‡] Concordia Pharmaceuticals, Inc.

[§] Ricerca Biosciences.

[a] Abbreviations: FTS, farnesyl thiosalicylic acid; FTS-A, FTS-amide; FTS-MA, FTS-methyl amide; FTS-DMA, FTS-dimethyl amide; FTS-ME, FTS-methyl ester; FTS-MOME, FTS-methoxymethyl ester; FTS-IE, FTS-isopropyl ester; FTS-BE, FTS-benzyl ester.

10.1021/jm801165r CCC: $40.75
Published on Web 12/15/2008

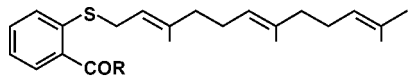

FTS: R=OH

FTS-ME: R=OCH_3

FTS-MOME: R=OCH_2OCH_3

FTS-IE: R=$OCH(CH_3)_2$

FTS-BE: R=$OCH_2C_6H_5$

FTS-A: R=NH_2

FTS-MA: R=$NHCH_3$

FTS-DMA: R=$N(CH_3)_2$

Figure 1. Structure of new FTS derivatives. Synthesis and purity of the compounds are detailed under Experimental procedures.

terms of inhibition of in vitro cell growth and Ras activity in human cancer cell lines. The most potent compound FTS-amide was then tested in vivo using nude mice tumor models.

Results

Synthesis and Chemical Characterization of New FTS Derivatives. The following derivatives were prepared: FTS-methylester (FTS-ME), FTS-methoxymethylester (FTS-MOME), FTS-isopropylester (FTS-IE), FTS-bezylester (FTS-BE), FTS-amide (FTS-A), FTS-methylamide (FTS-MA), and FTS-dimethylamide (FTS-DMA). The synthesis descriptions and purity of the compounds are detailed in Experimental procedures. Structures of the compounds are shown in Figure 1.

Effects of FTS Derivatives on Growth of Human Cancer Cell Lines. Our first goal was to establish efficacy of the new compounds in cell growth assays. We performed in vitro growth inhibition assays using a cancer cell line that harbors an oncogenic K-Ras, the pancreatic cell line Panc-1, and a cell line in which Ras is not mutated but is chronically active due to high activity of growth factor receptors, the glioblastoma cell line U87. The cells were incubated with and without each drug for 5 days, and cell number was then determined by direct counting (see Experimental Section). First we examined the effects of the FTS-ester derivatives on Panc-1 (Figure 2A) and on U87 cells (Figure 2C). All of the esters caused a dose-dependent decrease in cell number at the concentration range of 6−100 μM. These effects were mainly due to inhibition of cell growth except for the higher dose where cell death was observed as well. FTS-MOME was the most potent growth inhibitor with an IC_{50} of 15 μM in both cell lines. FTS-ME was somewhat less effective in Panc-1 cells (IC_{50} = 30 μM) but exhibited the same growth inhibition potency as FTS-MOME in U87 cells (Figure 2C, Table 1). FTS-IE and FTS-BE were clearly less potent than the two other esters with an IC_{50} > 50 μM in both cell lines (Figure 2A,C, Table 1).

Next, we examined the effects of the FTS-amides on panc-1 and U87 cells (Figure 2C,D). All three FTS amide derivatives caused a dose-dependent decrease in cell number of both cell lines at the concentration range of 6−100 μM exhibiting similar potencies (Figure 2B,D). Cell death was observed at concentrations higher than 50 μM. The IC_{50}s recorded in both cell lines were at the range of 10−20 μM (Table 1). Interestingly, five of the seven new compounds were more effective growth inhibitors of Panc-1 and U87 cells as compared to FTS whose reported IC_{50} values 35 μM in Panc-1[34] and 50 μM in U87 cells.[26]

Altogether, these results demonstrate that certain modifications on the carboxyl group of FTS yield active compounds capable, to various degrees, of inhibiting cancer cell growth. Moreover, some of the modifications, namely addition conversion of FTS to its methyl ester, methoxymethyl ester, amide, methyl amide, and dimethyl amide derivatives, showed improved efficacy as compared to FTS in inhibiting tumor cell growth. On the other hand, the benzyl ester or isopropyl ester showed a decrease in growth inhibition as compared to FTS itself.

Effect of FTS Derivatives on Ras and Its Downstream Effectors ERK and Akt. We next wanted to examine whether the growth inhibitory effects exerted by the FTS derivatives were associated with down regulation of Ras signaling, as in the case of FTS.[25,26,28,35] We thus used the Ras-GTP pull down assay (see Experimental procedures) and examined the effects of the more potent compounds on the levels of all three Ras isoforms. Typical immunoblots demonstrating the effect of FTS-A on the level of all active Ras isoforms (total Ras-GTP) and on the levels of the individual active K-Ras-GTP, H-RasGTP, and N-Ras-GTP in Panc-1 and U87 cells are shown in Figure 3. As shown, FTS-A caused a clear decrease in the levels of total Ras-GTP as well as in K-Ras-GTP in both cell lines. Reduction in the level of N-Ras-GTP was observed only in U87 cells, and no effect on H-Ras-GTP was observed in either cell line (Figure 3). Table 2 summarizes the results obtained with FTS-ME, FTS-MOME, FTS-A, FTS-MA, and FTS-DMA. As shown, FTS-A, FTS-MA, and FTS-DMA caused a clear decrease in the levels of K-Ras-GTP in Panc-1 cells (respectively 56.3 ± 11.2%, 52.3 ± 12.6%, and 47.8 ± 12.4% inhibition) and in U87 cells (respectively 50.8 ± 9.2%, 32.6 ± 9.4%, and 28 ± 16.5% inhibition). Reduction in the level of N-Ras-GTP was observed only in U87 cells; the degree of inhibition by FTS-A, FTS-MA, and FTS-DMA was respectively 37.3 ± 8.9%, 22.5 ± 6.5%, and 41 ± 4.6%. No effect on H-Ras-GTP was observed in either cell line (Table 2). However, FTS-ME and FTS-MOME, the more potent growth inhibitors among the ester derivatives, unexpectedly had a lesser effect on Ras-GTP in either cell line. Together these results suggested that only the FTS-amide derivatives mimicked the effect of the parental compound FTS, while the growth inhibition activity of the FTS esters may include a mechanism beyond Ras inhibition. That is to say, the amide derivatives of FTS exhibited both growth inhibitory activity and affected the target active Ras protein; the oncogenic K-Ras in Panc-1 cells and the chronically active N-Ras and K-Ras in U87 cells. Consistent with this notion, we found that in U87 cells FTS-A caused a significant decrease in the level of phospho-ERK and phospho-AKT, two classical downstream effectors of Ras (Figure 3). The impact of FTS-A on these signaling molecules in Panc-1 cells was less pronounced, presumably because under the conditions used these pathways were not active.

We have considered the possibility that ester or amide hydrolysis could have occurred under the culture conditions used, leading to the formation of FTS itself. Our results do not support this possibility. First, both FTS-A and FTS-ME exhibited a significantly higher growth inhibitory activity as compared with FTS (Table 1); if they were hydrolyzed, then these compounds would have exhibited potency similar to FTS. A significantly higher uptake of the FTS derivatives is also unlikely in light of previous experiments that demonstrated that cells take up farnesylated peptides with very high efficiency.[36] Second, FTS-ME exhibited different pharmacology than FTS (Table 2); if it was hydrolyzed to FTS, we would have detected a stronger effect of FTS-ME on Ras-GTP as compared with FTS, but this was not the case (Table 2). Third, our next set of

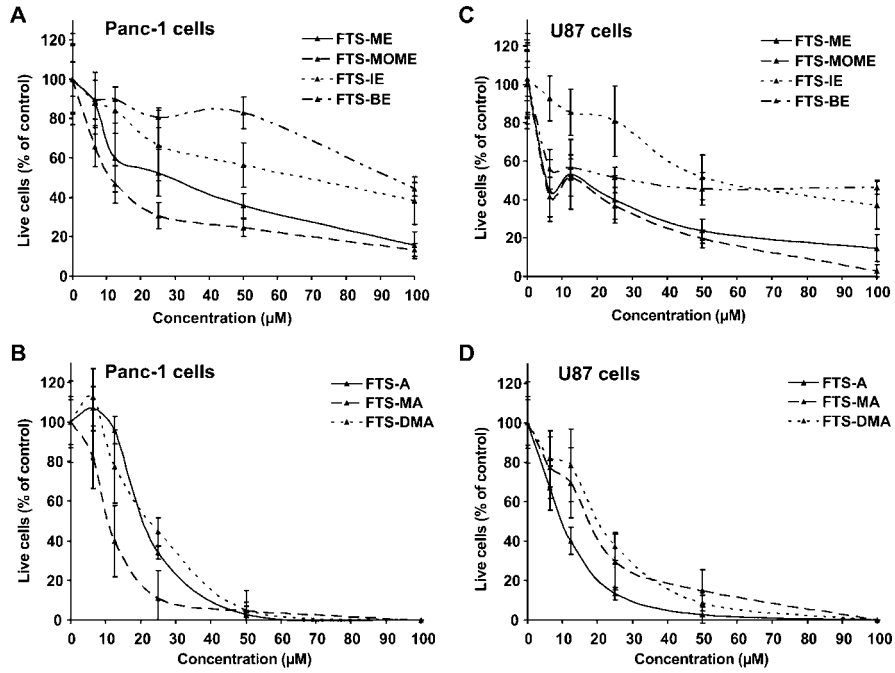

Figure 2. Inhibition of cell growth by FTS derivatives. Panc-1 and U87 cells were seeded in 24 wells plates at a density of 5000 cells/well. After 24 h, the media were replaced with media containing either the detailed FTS derivatives (6.25, 12.5, 25, 50, and 100 μM) or the control vehicle (0.1% DMSO). Five days later, the cells were collected and counted. Growth inhibition curves are presented for: (A) Panc-1 cells treated with FTS-ME, FTS-MOME, FTS-IE, and FTS-BE; (B) Panc-1 cells treated with FTS-A, FTS-MA, and FTS-DMA; (C) U87 cells treated with FTS-ME, FTS-MOME, FTS-IE, and FTS-BE; (D) U87 cells treated with FTS-A, FTS-MA, and FTS-DMA. The values shown are from 2 independent experiments (means $\pm$ SD, $n = 8$).

Table 1. IC_{50} Values of FTS Derivatives in Panc-1 and U87 Cells[a]

	IC_{50} (μM)	
FTS derivatives	Panc-1	U87
FTS[b]	35	50
FTS-ME	30	10
FTS-MOME	12	10
FTS-IE	70	52
FTS-BE	95	30
FTS-A	20	10
FTS-MA	10	18
FTS-DMA	22	20

[a] The IC_{50} values of the detailed FTS derivatives were calculated from the growth inhibitory curves shown in Figure 2. [b] The IC_{50} of FTS was previously calculated for Panc-1 cells[34] and for U87 cells.[26]

pharmacokinetic experiments as described bellow confirmed that FTS-A is indeed stable.

Altogether, these experiments suggested that FTS-amides act like FTS as Ras inhibitors. FTS-A seemed to exhibit a relatively higher activity as compared with FTS (about 3−5 times more potent) and thus was employed in the subsequent animal experiments.

Pharmacokinetics of FTS-Amide. First, we evaluated the pharmacokinetics of FTS-A after oral gavage administration (100 mg/kg) using rats as a model (see Experimental Section). Following dosing, blood samples were collected at the indicated times (10−330 min). Samples were then processed and analyzed by LC-MS/MS as described in the Experimental Section. A calibration curve for FTS-A was prepared ranging from 1 to 2500 ng/mL and was linear over this range. FTS-A was readily detected in rat plasma by LC-MS/MS at a detection limit of 1 ng/mL. Compared with the expected retention time of the parent ion (FTS-A, 1.01−1.02 min), the retention times of the tested sample ions was 1.02 min, corroborating the assay method and confirming that the compound remains stable in the plasma (Figure 4A). Plasma concentration curves for FTS-A at the

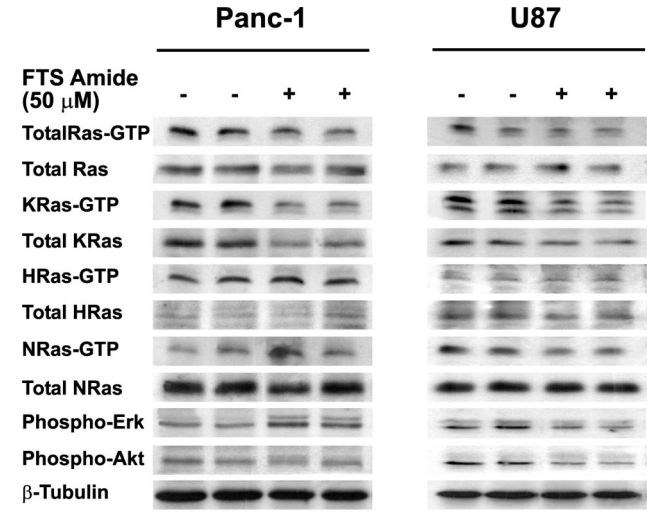

Figure 3. Effect of FTS-A on Ras signaling. Panc-1 and U87 cells were seeded at a density of 1.5×10^6 cells per 10-cm plate. After 24 h, the media were replaced with media containing either FTS-A (50 μM) or the control vehicle (0.1% DMSO) for 24 h. The cells were then lysed, and aliquots of the lysates were immunoblotted with anti pan-Ras, anti K-Ras, anti H-Ras, anti N-Ras, anti phospho-Akt, anti phospho-ERK, and anti β-tubulin antibodies. Total Ras-GTP, K-Ras-GTP, H-Ras-GTP, and N-Ras-GTP in the aliquots were determined by pull-down assays as described in Experimental Section. Typical immunoblots are shown for Panc-1 cells (left panel) and U87 cells (right panel).

various time points (Figure 4B) were used to calculate the pharmacokinetic variables by a noncompartmental model as detailed in the Experimental Section. The results thus obtained, namely the terminal-phase half-time (elimination half-time, $t_{1/2}$), the time at which the maximum plasma concentration (C_{max}) was reached (T_{max}), the C_{max}, and the area under the plasma concentration-time curve (AUC), are summarized in Table 3

Table 2. Inhibition of Active Ras by FTS Derivatives[a]

	% inhibition of active Ras levels							
	Panc-1				U87			
FTS derivatives	total Ras-GTP	KRas-GTP	NRas-GTP	HRas-GTP	total Ras-GTP	KRas-GTP	NRas-GTP	HRas-GTP
FTS-ME	5.3 ± 4.1	11.9 ± 13.8				23.8 ± 18.6	18.7 ± 2.8	
FTS-MOME	2.6 ± 3.8	19.9 ± 41.2				4.8 ± 14.8	5.1 ± 23.6	
FTS-A	37.4 ± 8.6[b]	56 ± 11.2[c]	8.6 ± 33.1		33 ± 12.7[b]	50.8 ± 9.2[c]	37.3 ± 8.9[b]	
FTS-MA	39.7 ± 6.1[c]	52 ± 12.6[c]	18.8 ± 19.3		34.7 ± 7.8[b]	32.6 ± 9.4[b]	22.5 ± 6.5[b]	
FTS-DMA	38.6 ± 6.3[c]	48 ± 12.4[c]	13.6 ± 7.1		45.4 ± 8.8[c]	28 ± 16.5[b]	41 ± 4.6[c]	14 ± 12.7

[a] Panc-1 and U87 cells were seeded at a density of 1.5×10^6 cells per 10-cm plate. After 24 h, the media were replaced with media containing either 50 μM of the FTS derivatives or the control vehicle (0.1% DMSO) for 24 h. The cells were then lysed and aliquots of the lysates were used to determine total Ras-GTP, K-Ras-GTP, H-Ras-GTP, and N-Ras-GTP levels by pull-down assays as described in Experimental Section. Protein bands were visualized by enhanced chemiluminescence and quantified by densitometry using EZQuant-Gel computer software. The percentage of active Ras inhibition was calculated as the subtraction of the percentage of active Ras levels after drug treatment (compared to control levels) from the percentage of active Ras levels in the control. Values are presented for Panc-1 cells (left panel) and U87 cells (right panel) as means ± SD. [b] $P < 0.05$. [c] $P < 0.01$.

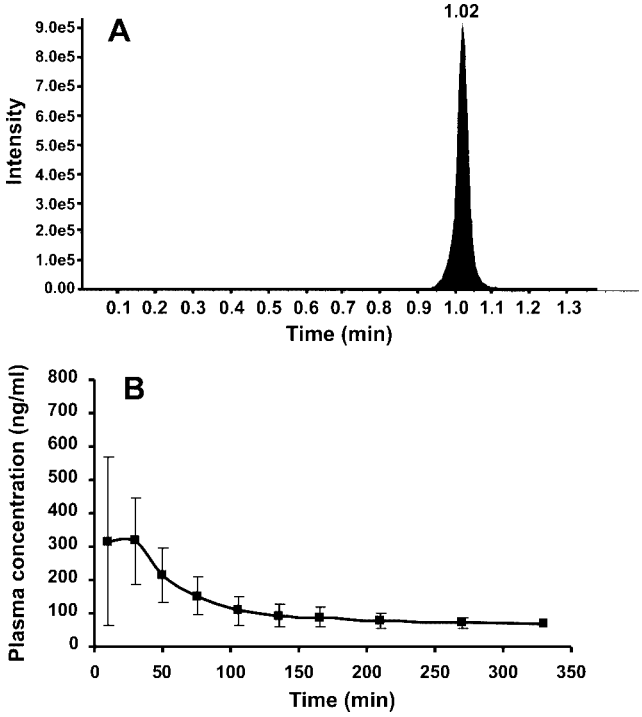

Figure 4. Plasma analysis for orally administered FTS-A. Animals received orally 100 mg/kg FTS-A in corn oil, and plasma samples were collected and analyzed by LC-MS/MS as detailed in the Experimental Section. (A) Typical chromatogram for FTS-A plasma analysis of a 50 min sample. (B) Plasma concentration curve for FTS-A was prepared using a calibration curve. Mean values (±SE, $n = 4$) determined at the indicated times are shown.

Table 3. Pharmacokinetic Parameters for FTS-A and FTS[a]

parameter	FTS-A	FTS[b]
dose (mg/kg)	100	40
half-life (min)	314	141.6
T_{max}	110	60
C_{max} (ng/mL)	371	2159.4
$AUC_{0\text{-inf}}$ (min·ng/mL)	108783	372432

[a] The pharmacokinetic parameters for FTS-A were calculated using the mean time/concentration data at 11 time points (10−330 min). [b] The pharmacokinetic parameters for FTS are from ref 27.

and compared to the previously obtained pharmacokinetic variables of FTS.[27] As shown in Table 3, although the $t_{1/2}$ value for FTS-A is more than 2-fold higher than that of FTS, its availability in the plasma is lower than that of FTS; the T_{max} value for FTS-A is almost 2-fold higher than that of FTS and the C_{max} and AUC values are significantly lower even though FTS-A was given at a higher dose than FTS.

FTS-Amide Inhibits Growth of Human Tumors in Nude Mouse Models. Next we examined the effect of FTS-A on brain tumor growth using a nude mouse model with human glioblastoma U87 cells implanted intracranially into the striatum area. Four days post-implantation, the mice were scanned by MRI to confirm tumor formation and were divided into two groups of seven control and seven drug-treated animals. Treatment started one day after the first MR imaging and subsequent MR imaging was performed on days 4, 9, and 13 following start of treatment. FTS-A (100 mg/kg) was administered orally twice daily (see Experimental Section). T_1- and T_2-weighted MR images were acquired after Gd-DTPA injection using the 7-T BioSpec magnet. The T_1-weighted images were used to measure tumor volume. The T_2-weighted images were used to obtain information about inflammation and ventricle enlargement. Figure 5A shows T_1-weighted MR images of representative control and FTS-A treated mice recorded before treatment (baseline images) and on day 4 (1st followup) and day 9 (2nd followup) after the treatment began. The T_1-weighted images of the control mouse demonstrate the rapid increase in tumor volume over time. The increase in tumor volume recorded over time in the FTS-A mouse was significantly lower than that recorded in the control mouse (Figure 5A). The data clearly imply that more contrast agent molecules accumulated in the control mice as compared to the FTS-A treated mice. Importantly, we did not observe any inflammatory response in the brains of the controls or in the brains of the drug-treated mice (not shown).

The T_1-weighted images were used to evaluate tumor volumes in the followups of all control and all drug-treated mice employing the MIA MATLAB program (see Experimental Section). The data were expressed in terms of "normalized tumor growth", namely the subtraction of the initial tumor volume from the tumor volume on the indicated followup divided by the initial tumor volume. The results of the analysis for followups 1 and 2 (days 4 and 9 of drug treatment) are presented in Figure 5B for the controls and FTS-A-treated mice. The mean value of the "normalized tumor growth" in the FTS-A treated mice ($n = 7$) was significantly smaller than that of the controls ($n = 7$) in both followups 1 and 2 (Mann−Whitney, * $P < 0.05$, ** $P < 0.01$) indicating respectively 80% and 50% inhibition (Figure 5B).

We also examined the impact of FTS-A on Panc-1 tumor growth in nude mouse models as described earlier.[27,34] Cells were implanted subcutaneously just above the right femoral joint of nude mice and oral treatment with FTS-A (100 mg/kg po, daily) began when palpable tumors were observed. Tumors were removed 18 days later and weighed. As shown in Figure 5C,

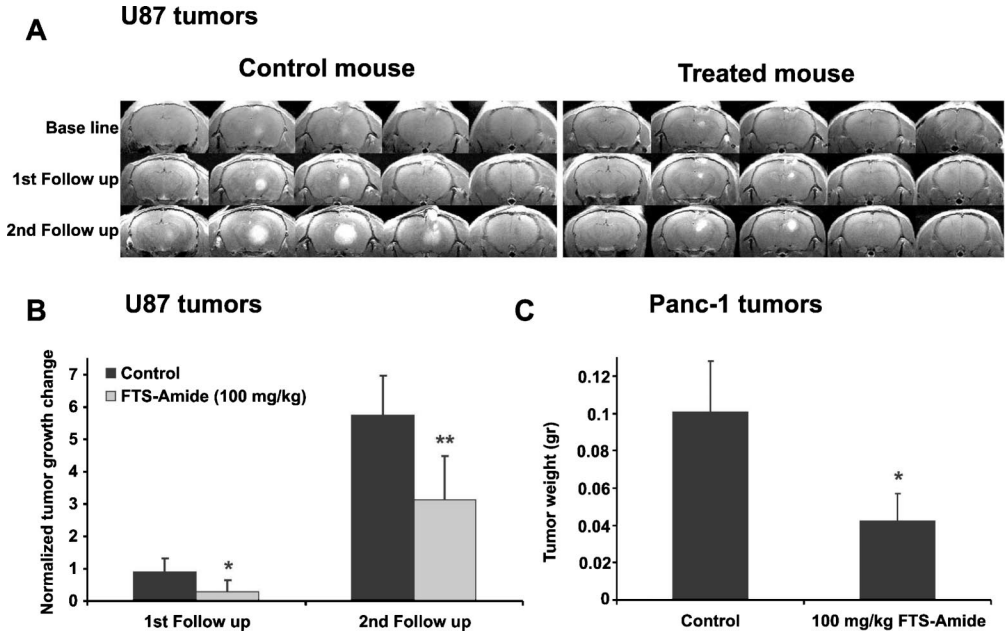

Figure 5. FTS-A inhibits growth of U87 and Panc-1 tumors in nude mice. U87 cells (5×10^5) were injected into the striata of nude mice (1 μL/min, 5 min total) as detailed in the Experimental Section. Four days later, the mice were MR imaged to verify tumor development and the mice were divided into two groups exhibiting similar tumor sizes. Starting from day 5, the mice were treated either with po dosing of 50 μL FTS-A (100 mg/kg) twice a day or with po doses of 50 μL vehicle solutions twice a day. Followup MR images were taken on days 9, 14, and 18. T_1-weighted images from the baseline imaging (day 4), first followup (day 9), and second followup (day 14) are shown in (A) for a typical control mouse (left panel) and a typical treated mouse (right panel). (B) Tumor volumes were measured from T_1-weighted MR images and the normalized ratio of tumor growth between followups was calculated as the subtraction of the initial tumor volume from the tumor volume in followup(n) divided by the initial tumor volume (mean $\pm$ SD, $n = 7$, * $P < 0.05$, ** $P < 0.01$). (C) Panc-1 cells (5×10^6) were injected subcutaneously just above the right femoral joint. Ten days later, tumors were measured and mice were divided into a treated group receiving daily po doses of 100 μL FTS-A (100 mg/kg) and a control group receiving daily po doses of 100 μL vehicle solution. Eighteen days later, the tumors were extracted and weighed as shown (mean $\pm$ SD, $n = 8$, * $P < 0.05$).

the average tumor weight in the treated group was more than 2-fold smaller than that of the control group (unpaired t test with Welch correction, * $P < 0.05$). In conclusion, it appears that oral FTS-A significantly attenuated both Panc-1 and U87 tumor growth in the nude mouse without causing any toxic side effects, making it an interesting new Ras inhibitor for potential treatment of Ras-dependent tumors.

Discussion

We have prepared and characterized new FTS derivatives in which the carboxyl group has been modified by esterification or amidation. We found that all of the FTS amides and two of the FTS esters (FTS-ME and FTS-MOME) strongly inhibited growth of Panc-1 and of U87 cells in which at least one Ras isoform is chronically active.[37,38] The esters FTS-IE and FTS-BE were far less active than FTS or the other compounds examined. This indicates that the bulky group (isopropyl and benzyl) of these esters may interfere with growth inhibitory activity of these FTS derivatives. FTS itself acts as a Ras inhibitor that inhibits Ras membrane anchorage by interfering with galectin-1- and galectin-3-induced nanoclustering of, respectively, the oncogenic H-Ras and K-Ras isoforms in the cell membrane.[21,22] This interference blocks the robust signaling of the Ras nanocluster. This seemed to be also the case of the new FTS-amides, which reduced the levels of active Ras in Panc-1 and in U87 cells. However, FTS esters, even those that exhibited relatively strong growth inhibitory activity, had a much reduced effect on Ras (Table 2). Therefore we suspect that the growth inhibitory action of the FTS-ester derivatives (FTS-ME and FTS-MOME) is a result of interference with Ras-independent cell growth pathways.

The lowered effect of FTS-ME on Ras is even more surprising in light of the knowledge that all Ras proteins possess a carboxy-terminal farnesylcysteine carboxy methyl ester.[16,18] Interestingly, like FTS, *N*-acetyl farnesylcystine (AFC), which mimics the carboxy terminal of Ras proteins, is also known to inhibit ERK activation.[39] However, AFC and FTS appear to differ in their modes of action on Ras proteins and on Icmt, the enzyme that methylates Ras proteins. AFC acts mostly as an inhibitor of the Icmt, serving actually as a competitive substrate of the enzyme.[40] FTS is a pure inhibitor of the Icmt enzyme and does not serve as a substrate for the enzyme.[41] At its growth inhibitory concentrations, (10−50 μM) FTS dislodges the active Ras from the cell membrane without an effect on methylation.[24,41] As has been discussed previously, AFC inhibits Ras methylation, thereby blocking Ras trafficking to the cell membrane,[39] while FTS dislodges the mature Ras from the cell membrane.[24] Nevertheless, when AFC, but not FTS, enters the cell, it inevitably becomes methylated, and thus AFC-methyl ester accumulates at the expense of AFC. When FTS enters the cell, it retains its free carboxyl group. Because we show here that the synthetic FTS-methyl ester has a diminished effect on Ras, we think that, similarly, AFC-methyl ester that accumulates in cells may not dislodge Ras from the cell membrane because it does not bind to Ras scaffolds such as galectin-1 and galectin-3. Accordingly, the more hydrophobic nature of FTS-ME and of AFC-methyl ester as compared to their free carboxylic acid derivatives might inhibit the interactions with Ras scaffolds. This, however, is not the case of the FTS-amides, which may accommodate better in the putative prenyl binding pockets of Gal-1[20] and Gal-3.[42]

The above observations strongly suggest that carboxyl methylated prenyl analogues, including FTS-ME or FTS-MOME, inhibit cell growth by interfering with prenyl binding proteins other than Ras escorts. It is tempting to speculate that FTS-ME or FTS-MOME would interfere with the action of the well-described prenyl binding proteins RhoGDIs that bind the geranylgeranyl isoprenoid moieties of Rac/Rho GTPases, known to be involved in cell growth and cell transformation.[43,44] Consistent with this suggestion are the results of experiments that determined the binding of isoprenylated acids to RhoGDI.[45] These experiments showed that isoprenylated carboxy methyl esters exhibit strong interactions with RhoGDI while their corresponding free carboxylic acid derivatives exhibit weak interactions with RhoGDI.[45] For example, AFC-methyl ester exhibited high affinity to RhoGDI while AFC and FTS barely interacted with RhoGDI.[45] Interestingly, the isoprenoid moiety of Rac/Rho GTPases accommodates precisely within a hydrophobic pocket in RhoGDI[43,44] and, indeed, *N*-acetyl geranylgeranyl cysteine binds strongly to RhoGDI.[45] Thus it seems that strong association of prenylated compounds with RhoGDI depends on both the length of the isoprenoid group and the carboxymethyl ester. Important questions that remain to be answered in future experiments include whether or not such compounds, as well as FTS-ME, block the hydrophobic pocket of RhoGDIs in vivo, and if so how does this affect cell growth. In light of the important functions of RhoGDIs as specific regulators of Rac/Rho GTPases trafficking to and from the cell membrane,[46] it is tempting to speculate that such blockage will result in miss localization and functioning of these GTPases. This would result in inhibition of cell growth.

The relatively strong anti-Ras activity of the FTS-amides, particularly of FTS-amide, suggests that amidation, unlike methylation, of the carboxyl group is favorable for the interactions with Ras escort proteins. So then, while methylation abrogated anti-Ras activity, amidation strengthened this activity. Importantly, FTS-amides retained the selectivity toward active Ras-GTP of the parental compound FTS. This was apparent in their inhibitory activities in Panc-1 and in U87 cells; in Panc-1 cells, the most prevalent active Ras isoform is K-Ras-GTP, as they express the oncogenic K-RasG12V.[37] Similarly, we showed previously that N-Ras-GTP and to a lesser extent K-Ras-GTP or H-Ras-GTP was inhibited by FTS in U87 cells.[26] Of all prenylated derivatives with anti-Ras activity, FTS-A (IC_{50} = 10 μM) appears to be the most potent inhibitor of active Ras described thus far.

We therefore examined the impact of FTS-A on tumor growth in animal models. We used an oral formulation to allow comparison with results obtained with oral FTS.[27] In the Panc-1 nude mouse model, FTS-A exhibited a potency that was comparable with that of FTS, namely, 100 mg/kg daily FTS-A caused a ~60% decrease in tumor weight, while in previous work, FTS (80 mg/kg, daily) caused approximately the same effect.[27] Similarly, in the intracranial U87 nude mouse model, treatment with oral FTS-A at daily dose of 100 mg/kg showed clear tumor growth inhibition (Figure 5). Here, too, the effect was not stronger than that observed with FTS in the same model (Goldberg et al. in preparation). Thus, in spite of the in vitro higher potency of FTS-A as compared with FTS, the in vivo effects of the two inhibitors were similar. This apparent discrepancy is clearly associated with differences in pharmacokinetics and pharmacodynamics of FTS-A and FTS. Although FTS-A exhibits a longer elimination half-time than FTS (Table 3), it seems to be less available than FTS in the plasma and therefore yields similar and not improved tumor growth inhibitory effects compared to FTS.

Conclusions

Our results along with previous studies that used prenylated small molecules[47,48] show that the structure of such molecules is a critical functional determinant. While FTS and its amide derivatives act as Ras inhibitors, FTS esters show lesser activity as Ras inhibitors and may interfere with the function of other prenyl-binding proteins such as RhoGDIs and thereby inhibit cell growth.

Experimental Section

Chemistry. The compounds prepared were FTS-methyl ester (FTS-ME), FTS-methoxy-methyl ester (FTS-MOME), FTS-isopropyl ester (FTS-IE), FTS-benzyl ester (FTS-BE), FTS-amide (FTS-A), FTS-methyl amide (FTS-MA), and FTS-dimethyl amide (FTS-DMA). Direct coupling of FTS with the appropriate amine, alcohol, or methoxymethychloride provided FTS-MOME, FTS-IE, FTS-BE, FTS-A, FTS-MA, and FTS-DMA. FTS-ME was prepared from methyl thiosalicylate and farnesol.

***S-trans,trans*-Farnesylthiosalicylamide (FTS-A).** A mixture of 9.0 g of *S-trans,trans*-farnesylthiosalicylic acid (FTS), 9.6 g of 1-ethyl-3-[dimethylaminopropyl]carbodiimide hydrochloride, 6.75 g of 1-hydroxybenzotriazole, 2.7 g of ammonium chloride, and 150 mL of dimethylformamide was sonicated for 5 min and then cooled in an ice bath under argon. Diisopropylethylamine, 12.95 g, was added dropwise with stirring at 0 °C, and the mixture was stirred at ice bath temperature for 2.5 h. Ethyl acetate was added, the mixture was washed with aqueous citric acid, aqueous sodium bicarbonate, and brine, and the organic layer was dried over anhydrous sodium sulfate and concentrated to yellow syrup. Trituration with hexane provided 12.9 g (87%) of off-white solid, purity ≥97%. ^{1}H NMR (300 MHz, DMSO-d_6) δ: 7.75 (bs, 1H), 7.43−7.33 (m, 4H), 7.22−7.12 (m, 1H), 5.25 (t, 1H), 5.06 (bt, 2H), 3.54 (d, 2H), 2.6−1.88 (m, 8H), 1.63 (s, 6H), 1.56 (s, 6H). LC/MS: (+) ESI m/z = 358 $[M + H]^+$; 380 $[M + Na]^+$.

***N*-Methyl-*S-trans,trans*-Farnesylthiosalicylamide (FTS-MA).** A mixture of 5.0 g of *S-trans,trans*-farnesylthiosalicylic acid (FTS), 80 mL of dichloromethane, 16.0 mL of methylamine, and 6.4 mL of triethylamine was stirred under argon, 6.8 g of benzotriazol-1-yl-oxy-tris-(dimethylamino)phosphonium hexafluorophosphate was added, and the mixture was stirred for 18 h at room temperature. The mixture was concentrated under reduced pressure to an oil, which was purified by flash chromatography, eluting with hexanes/ethyl acetate (9/1−3/7) to provide 5.18 g (99%) of yellow oil, purity ≥98%. ^{1}H NMR (300 MHz, $CDCl_3$) δ: 7.70 (dd, 1H), 7.33 (m, 3H), 6.85 (s, 1H), 5.26 (t, 1H), 5.06 (m, 2H), 3.53 (d, 2H), 3.02 (d, 3H), 2.02 (m, 8H), 1.68 (s, 3H), 1.59 (s, 3H), 1.58 (s, 6H). LC/MS: (+) ESI m/z = 372 $[M + H]^+$; 394 $[M + Na]^+$.

***N,N*-Dimethyl-*S-trans,trans*-Farnesylthiosalicylamide (FTS-DMA).** A mixture of 5.0 g of *S-trans,trans*-farnesylthiosalicylic acid (FTS), 80 mL of dichloromethane, 16.0 mL of dimethylamine, and 6.4 mL of triethylamine was stirred under argon, 6.8 g of benzotriazole-1-yl-oxy-tris-(dimethylamino)phosphonium hexafluorophosphate was added, and the mixture was stirred for 18 h at room temperature. The mixture was concentrated under reduced pressure to an oil, which was purified by flash chromatography, eluting with hexanes/ethyl acetate (9/1−3/7) to provide 5.19 g (96%) of a pale-yellow oil, purity ≥99%. ^{1}H NMR (300 MHz, $CDCl_3$) δ: 7.39 (dd, 1H), 7.27 (m, 3H), 5.28 (t, 1H), 5.08 (bm, 2H), 3.56 (d, 2H), 3.14 (s, 3H), 2.83 (s, 3H), 1.68 (s, 3H), 1.60 (s, 3H), 1.59 (s, 6H). LC/MS: (+) ESI m/z = 386 $[M + H]^+$; 408 $[M + Na]^+$.

Methyl *S-trans,trans*-Farnesylthiosalicylate (FTS-ME). A solution of 7.0 g of *trans,trans*-farnesol, 63 mL of tetrahydrofuran, and 5.7 mL of triethylamine was cooled to −50 °C. With stirring under argon, a solution of 2.9 mL of methanesulfonyl chloride in

21 mL of tetrahydrofuran was added dropwise over 30 min, and the mixture was stirred for 2.5 h at −50 °C. Then a solution of 4.3 mL of methyl thiosalicylate, 42 mL of tetrahydrofuran, and 4.4 mL of triethylamine was added dropwise with stirring at −50 °C, the mixture was stirred at −50 °C for 2.5 h, and at 0 °C for 12 h. The mixture was filtered and concentrated to a syrup, which was partitioned between chloroform and 2% hydrochloric acid. The chloroform layer was washed with water, dried over sodium sulfate, and concentrated to an oil, which was purified on a filter pad of flash silica, eluting with hexanes/ethyl acetate (80/1−40/1) to provide 7.2 g (62%) of colorless oil, purity ≥96%. ^{1}H NMR (300 MHz, $CDCl_3$) δ: 7.95 (dd, 1H), 7.42 (td, 1H), 7.31 (d, 1H), 7.15 (t, 1H), 5.34 (bt, 1H), 5.09 (bt, 2H), 3.91 (s, 3H), 3.58 (d, 2H), 2.1−2.0 (m, 6H), 1.9−1.8 (m, 2H), 1.73 (s, 3H), 1.68 (s, 3H), 1.60 (s, 6H). LC/MS: (+) ESI m/z = 373 $[M + H]^+$; m/z = 395 $[M + Na]^+$.

Isopropyl *S-trans,trans*-Farnesylthiosalicylate (FTS-IE). To a stirred solution of 6.39 g of *S-trans,trans*-farnesylthiosalicylic acid (FTS), 2.61 g of dimethylaminopyridine, and 162 mL of dichloromethane was added 4.78 g of dicyclohexyldiimide. Then 4.09 mL of isopropyl alcohol was added, and the mixture was stirred at ambient temperature overnight. The mixture was filtered, and the filtrate was concentrated to an oil, which was chromatographed on a filterpad of flash silica, eluting with hexanes/ethyl acetate (20/1) to provided 5.88 g (83%) of colorless oil, purity ≥98%. ^{1}H NMR (300 MHz, $CDCl_3$) δ: 7.93 (dd, 1H), 7.40 (td, 1H), 7.31 (d, 1H), 7.14 (td, 1H,), 5.34 (t, 1H), 5.26 (m, 1H), 5.09 (t, 2H), 3.57 (d, 2H), 2.05 (m, 6H), 1.98 (m, 2H), 1.72 (s, 3H), 1.68 (s, 3H), 1.60 (s, 6H), 1.37 (s, 6H). LC/MS (+) ESI: m/z 401 $[M + H]$;[1] m/z 423 $[M + Na]^+$.

Benzyl *S-trans,trans*-Farnesylthiosalicylate (FTS-BE). To a solution of 7.50 g of *S-trans,trans*-farnesylthiosalicylic acid (FTS), 3.06 g of dimethylaminopyridine, and 189 mL of dichloromethane was added with stirring 5.61 g of dicyclhexylcarbodiimide. Then 4.76 mL of benzyl alcohol was added, and the mixture was stirred at ambient temperature overnight. The mixture was filtered, and the filtrate concentrated to an oil, which was dissolved in ether. The ether solution was washed with 2% hydrochloric acid and brine, dried over sodium sulfate, and concentrated to an oil, which was chromatographed on a filterpad of flash silica, eluting with hexanes/ethyl acetate (20/1) to afford 6.85 g (73%) of colorless oil, purity ≥98%. ^{1}H NMR (300 MHz, $CDCl_3$) δ: 8.00 (dd, 1H), 7.47−7.30 (m, 7H),7.13 (t, 1H), 5.35 (m, 1H), 5.09 (bt, 2H), 3.58 (d, 2H, 2.08−1.96 (m, 8H), 1.72 (s, 3H), 1.68 (s, 3H), 1.60 (s, 6H). LC/MS (+) ESI: m/z = 449 $[M + H]^+$; m/z = 471 $[M + Na]^+$.

Methoxymethyl *S-trans,trans*-Farnesylthiosalicylate (FTS-MOME). To a flask containing 0.264 g of sodium hydride under argon was added with stirring 1 mL of hexamethylphosphoramide. With cooling, a solution of 3.59 *S-trans,trans*-farnesylthiosalicylic acid (FTS) in 10 mL of hexamethylphosphoramide was added dropwise over 30 min, and the mixture was stirred at room temperature for 30 min. In one portion, 0.84 mL of chloromethyl methyl ether was added and stirring was continued for 3 h. The mixture was poured into saturated aqueous sodium carbonate and extracted with ether. The ether solution was washed with water and brine, dried over sodium sulfate, and concentrated to an oil, which was chromatographed on a filterpad of flash silica, eluting with hexanes/ethyl acetate (20/1) to provide 3.1 g (78%) of colorless oil, purity ≥99%. ^{1}H NMR (300 MHz, $CDCl_3$) δ: 8.03 (dd, 1H), 7.45 (t, 1H), 7.33 (d, 1H), 7.17 (td, 1H), 5.49 (s, 2H), 5.34 (bt, 1H), 5.09 (bt, 2H), 3.59 (d, 2H), 3.56 (s, 3H), 2.1−2.0 (m, 6H), 1.99−1.96 (m, 2H), 1.73 (s, 3H), 1.68 (s, 3H), 1.59 (s, 6H). LC/MS (+) ESI: m/z 425 $[M + Na]^+$.

Preparation of Compounds for the Experiments. The compounds were dissolved in chloroform to yield 0.1 M solutions of each. Aliquots (10 or 20 μL) of the solutions were kept at −70 °C. For each experiment, the chloroform was evaporated by a stream of nitrogen, and the compound was dissolved in 100% DMSO to yield a 0.1 M solution. This solution was diluted 1:1000 in DMEM/10%FCS to yield a 100 μM solution, which was then serially diluted with DMEM/10%FCS/0.1% DMSO to yield solutions containing 50, 25, 12.5, and 6.25 μM of each compound, which were then used in the experiments. For in vivo experiments, FTS-A was weighed and dissolved in corn oil to a concentration of 100 mg/kg. The vehicle control was corn oil.

Pharmacokinetic Sampling and Analysis. Assay development and plasma concentration determinations were conducted by NoAb BioDiscoveries. Four animals (male Sprague−Dawley rats, 275−285 g) were used to collect samples at each time point (10, 30, 50, 75, 105, 135, 165, 210, 270, and 330 min) taken after a single dose of 100 mg/kg FTS-amide, po. Approximately 0.2 mL of blood was collected in sodium heparin containing tubes via the femoral artery while under anesthesia (urethane/chloralose, 33%/1% w/v) at each of the specified collection times. The blood samples were immediately placed on ice and centrifuged (6800 rpm for 5 min at 4 °C) within 5 min of collection. Plasma was then collected and immediately stored at −70 °C. Peak plasma concentration, time peak achieved, and half-life (C_{max}, t_{max}, and $t_{1/2}$) were calculated. Area under the plasma concentration−time curves (AUC) was also determined. These analyses were conducted using Win-Nonlin (Phasight Corp).

Preparation of Calibration Standards and Extraction of Plasma for Analysis. Calibration standards of FTS-amide in rat plasma were prepared at 1, 5, 25, 125, 1250, and 2500 ng/mL. A sample (60 μL) of each calibration standard or plasma was mixed with 2 μL of the internal standard (17.5 μL/mL propanolol in acetonitrile) and then vortex mixed with 600 μL of acetonitrile to precipitate proteins. The samples were then centrifuged at 12000 rpm and 4 °C for 5 min. the supernatant was then transferred to glass tubes and evaporated to dryness under nitrogen at 40 °C. The residue was reconstituted with 60 μL of mobile phase (90%/10% of acetonitrile/5 mM ammonium acetate with 0.05% formic acid) and vortexed well. The precipitated samples were then centrifuged at 12000 rpm and 4 °C for 5 min and transferred into auto sampler vials.

Liquid Chromatography. Sample analysis was performed using a PE Sciex API 4000 Q-TRAP LC-MS/MS system equipped with an Agilent LC system with a binary pump and solvent degasser, an auto sampler, and a divert valve (VIVI, Valco Instrument Co. Inc.) installed between the column and the mass spectrometer inlet. An Onyx Monolithic C-18, 100 mm × 3.0 mm column was used. Mobile phase was acetonitrile/5 mM ammonium acetate with 0.05% formic acid (90/10, isocratic elution) at a flow rate of 1 mL/min, and the injection volume was 10 μL. Propanolol was used as an internal standard (IS). A sample cleanup method for plasma spiked with the test compound was developed using protein precipitation. Method qualification included: the determination of the ion transition for the compound and the IS (i.e., identification of the parent and daughter ions), determination of the linear dynamic range using five calibration standards (1−2500 ng/mL) in duplicate, and the evaluation of assay performance determined at three quality control (low, medium, and high) samples in duplicate.

Cell Cultures. Human glioblastoma U87 cells and Panc-1 cells (ATCC) were grown in Dulbecco's modified Eagle medium (DMEM) containing 10% fetal calf serum (FCS), 2 mM L-glutamine, 100 U/mL penicillin, and 100 μg/mL streptomycin. The cells were incubated at 37 °C in a humidified atmosphere of 95% air and 5% CO_2.

Growth Inhibition Experiments. U87 and Panc-1 cells were plated in 24-well plates at a density of 5000 cells per well and grown for 24 h. The medium was then replaced by a medium containing the indicated concentration of each compound or by a medium containing 0.1% DMSO (vehicle control). The cells were maintained in culture for 5−7 days and then counted. Data are expressed in terms of percentage: (number of cells in the drug treated culture/number of cells in the control × 100). Each experiment was performed twice in quadruplicates and the means ± SD are presented.

Western Immunoblotting. U87 or Panc-1 cells were plated at a density of 1.5 × 10^6 cells in 10-cm dishes, and were allowed to grow overnight in medium containing 10% FCS. The medium was then replaced by a medium containing either 50 μM of each

compound or 0.1% DMSO, and the cells were incubated for 24 h in the presence of the drugs. We then lysed the cells with solubilization buffer (50 mmol/L Tris-HCl (pH 7.6), 20 mmol/L $MgCl_2$, 200 mmol/L NaCl, 0.5% NP40, 1 mmol/L DTT, and protease inhibitors). Lysates were used to determine the Ras-GTP content by the glutathione *S*-transferase (GST)-RBD (Ras-binding domain of Raf) pull-down assay, followed by Western immunoblotting with mouse anti pan-Ras antibody (1:2500) or with Ras-isoform specific antibodies (mouse anti-H-Ras, anti-K-Ras, and anti N-Ras (1:100, Calbiochem) as described elsewhere.[49] Levels of total Ras proteins, phosphor-extracellular signal-regulated kinase (ERK), phospho-Akt, and β-tubulin in the cell lysates were determined by immunoblotting using the above anti-Ras antibodies, rabbit antiphospho-ERK1/2 antibody (1:10000, Sigma-Aldrich), rabbit antiphospho-Akt antibody (1:200, Cell Signaling), and rabbit anti β-tubulin (1:1000, Santa Cruz Biotechnology). Immunoblots were exposed either to peroxidase-goat antimouse IgG or peroxidase-goat antirabbit IgG (1:2500) accordingly. Protein bands were visualized by enhanced chemiluminescence and quantified by densitometry using EZQuant-Gel computer software.

Tumor Implantation. Nude CD_1-Nu mice (25−30 g) were housed in barrier facilities on a 12 h light/dark cycle. Food and water were supplied ad libitum. On day zero, Panc-1 cells (5×10^6 cells in 0.1 mL) were implanted subcutaneously just above the right femoral joint. On day 10, the tumors were measured and the mice were divided into treated and control groups. The treated animals received daily po doses of 100 μL FTS-amide (100 mg/kg), while the control animals received daily po doses of 100 μL vehicle solution. Approximately 18 days later, the tumors were extracted and weighed.

For intracranial tumor implantation, mice were anesthetized by intraperitoneal injection of ketamin (100 mg/kg) and xylazine hydrochloride (10 mg/kg) solution in 0.1 mL of PBS. Cell inoculation was performed on day zero by creating a mid-skull incision, and then a burr hole 1 mm lateral and 1 mm posterior to the bregma, 3 mm deep, into the striatum area. U-87 cells (0.5×10^6) were injected using a 1 mL of BASI gastight syringe connected to a pump, thus allowing slow release of the cells into the brain (1 μL/min, 5 min total). The mice were imaged on day 4 to verify tumor development as detailed in MRI procedures, and the mice were divided into two groups exhibiting similar tumor sizes. Drug treatments started on day 5: the treated group received po dosing of 50 μL of FTS-amide (100 mg/kg) twice a day, while the control animals received po doses of 50 μL vehicle solutions twice a day. Followup MR images were taken on days 9, 14, and 18.

MRI Procedures. In all MRI experiments, the mice were anesthetized with isofluorane (5% for induction, 1−3% for maintenance) in 1 L/min oxygen. Ten minutes before the MR imaging, the mice were injected with 0.1 mL of gadolinium diethylenetriaminepentaacetic acid (Gd-DTPA, Magnetol, Soreq Radiopharmaceuticals, Yavne, Israel) solution (0.05M). Once anesthetized, the animals were installed in a head-holder to ensure reproducible positioning inside the probe. Rate of respiration was monitored and was 60−80 breaths min^{-1} throughout the experimental period.

We used a 7 T BioSpec Magnet 70/30 USR system (Bruker, Germany) equipped with gradient coil system capable of producing pulse gradient of up to 40 gauss/cm in each of the three directions. The MRI protocol included transverse T_1- and T_2-weighted MR images. The T_1-weighted images were acquired using the spin−echo imaging sequence with a repetition delay (TR) of 800 ms, an echo delay (TE) of 12 ms, matrix dimension of 256 × 128 (interpolated to 256 × 256), and two averages, corresponding to an image acquisition time of 3 min 24 s. The T_2-weighted images were acquired using the RARE sequence with a TR of 3000 ms, TE effective of 50 ms, 256 × 128 matrix (interpolated to 256 × 256), RARE factor of 8, and four averages, corresponding to an image acquisition time of 3 min 12 s. Then 14 continuous slices with slice thickness of 1 mm were acquired with a field of view (FOV) of 2 cm × 2 cm.

Image processing was as follows: The tumor volume was calculated from the T_1-weighted MR images using the Medical Image Analysis (MIA version 2.4), MATLAB image processing toolbox. The normalized tumor growth between the follow-ups was calculated as detailed in the equation below for each animal and the results were averaged for each treatment group.

$$\text{normalized tumor growth change} = \frac{\text{tumor volume(follow-up}(n)) - \text{tumor volume(follow-up 1)}}{\text{tumor volume(follow-up 1)}}$$

Acknowledgment. We thank the Alfredo Federico Strauss Center for Computational NeuroImaging of Tel Aviv University. The MRI scanner used in this study was purchased with grants from The Israel Science Foundation (ISF) and the Raymond and Beverly Sackler Institute of Biophysics of Tel Aviv University. Y.K. is the incumbent of the Jack H. Skirball Chair in Applied Neurobiology. Grant support: supported in part by The Wolfson Foundation and by the Prajs-Drimmer Institute for the Development of Anti-Degenerative Disease Drugs

Supporting Information Available: Elemental analyses of new farnesylthiosalicylic acid derivatives. This material is available free of charge via the Internet at http://pubs.acs.org.

References

(1) Barbacid, M. Ras genes. *Annu. Rev. Biochem.* **1987**, *56*, 779–827.
(2) Boguski, M. S.; McCormick, F. Proteins regulating Ras and its relatives. *Nature* **1993**, *366*, 643–654.
(3) Bos, J. L. p21ras: an oncoprotein functioning in growth factor-induced signal transduction. *Eur. J. Cancer* **1995**, *31*, 1051–1054.
(4) Casey, P. J.; Solski, P. A.; Der, C. J.; Buss, J. E. p21ras is modified by a farnesyl isoprenoid. *Proc. Natl. Acad. Sci. U.S.A* **1989**, *86*, 8323–8327.
(5) Hancock, J. F.; Cadwallader, K.; Paterson, H.; Marshall, C. J. A CAAX or a CAAL motif and a second signal are sufficient for plasma membrane targeting of ras proteins. *EMBO J.* **1991**, *10*, 4033–4039.
(6) Hancock, J. F.; Magee, A. I.; Childs, J. E.; Marshall, C. J. All ras proteins are polyisoprenylated but only some are palmitoylated. *Cell* **1989**, *57*, 1167–1177.
(7) Kato, K.; Cox, A. D.; Hisaka, M. M.; Graham, S. M.; Buss, J. E.; Der, C. J. Isoprenoid addition to Ras protein is the critical modification for its membrane association and transforming activity. *Proc. Natl. Acad. Sci. U.S.A* **1992**, *89*, 6403–6407.
(8) Leevers, S. J.; Paterson, H. F.; Marshall, C. J. Requirement for Ras in Raf activation is overcome by targeting Raf to the plasma membrane. *Nature* **1994**, *369*, 411–414.
(9) Stokoe, D.; MacDonald, S. G.; Cadwallader, K.; Symons, M.; Hancock, J. F. Activation of Raf as a result of recruitment to the plasma membrane. *Science* **1994**, *264*, 1463–1467.
(10) Goldberg, L.; Kloog, Y. A Ras Inhibitor Tilts the Balance between Rac and Rho and Blocks PI3-Kinase-Dependent Glioblastoma Cell Migration. *Cancer Res.* **2006**, *66*, 11709–11717.
(11) Joneson, T.; White, M. A.; Wigler, M. H.; Bar Sagi, D. Stimulation of membrane ruffling and MAP kinase activation by distinct effectors of RAS. *Science* **1996**, *271*, 810–812.
(12) Walsh, A. B.; Bar-Sagi, D. Differential activation of the Rac pathway by Ha-Ras and K-Ras. *J. Biol. Chem.* **2001**, *276*, 15609–15615.
(13) Downward, J. Ras signalling and apoptosis. *Curr. Opin. Genet. Dev.* **1998**, *8*, 49–54.
(14) Scheffzek, K.; Ahmadian, M. R.; Kabsch, W.; Wiesmuller, L.; Lautwein, A.; Schmitz, F.; Wittinghofer, A. The Ras-RasGAP complex: structural basis for GTPase activation and its loss in oncogenic Ras mutants. *Science* **1997**, *277*, 333–338.
(15) Bos, J. L. Ras oncogenes in human cancer: a review. *Cancer Res.* **1989**, *49*, 4682–4689.
(16) Cox, A. D.; Der, C. J. Protein prenylation: more than just glue. *Curr. Opin. Cell Biol.* **1992**, *4*, 1008–1016.
(17) Marshall, C. J. Ras effectors. *Curr. Opin. Cell Biol.* **1996**, *8*, 197–204.
(18) Cox, A. D.; Hisaka, M. M.; Buss, J. E.; Der, C. J. Specific isoprenoid modification is required for function of normal, but not oncogenic, Ras protein. *Mol. Cell. Biol.* **1992**, *12*, 2606–2615.
(19) Elad-Sfadia, G.; Haklai, R.; Ballan, E.; Gabius, H. J.; Kloog, Y. Galectin-1 augments Ras activation and diverts Ras signals to Raf-1 at the expense of phosphoinositide 3-kinase. *J. Biol. Chem.* **2002**, *277*, 37169–37175.
(20) Rotblat, B.; Niv, H.; Andre, S.; Kaltner, H.; Gabius, H. J.; Kloog, Y. Galectin-1(L11A) predicted from a computed galectin-1 farnesyl-

binding pocket selectively inhibits Ras-GTP. *Cancer Res.* **2004**, *64*, 3112–3118.
(21) Elad-Sfadia, G.; Haklai, R.; Balan, E.; Kloog, Y. Galectin-3 augments K-Ras activation and triggers a Ras signal that attenuates ERK but not phosphoinositide 3-kinase activity. *J. Biol. Chem.* **2004**, *279*, 34922–34930.
(22) Belanis, L.; Plowman, S. J.; Rotblat, B.; Hancock, J. F.; Kloog, Y. Galectin-1 is a novel structural component and a major regulator of h-ras nanoclusters. *Mol. Biol. Cell* **2008**, *19*, 1404–1414.
(23) Marciano, D.; Ben Baruch, G.; Marom, M.; Egozi, Y.; Haklai, R.; Kloog, Y. Farnesyl derivatives of rigid carboxylic acids—inhibitors of ras-dependent cell growth. *J. Med. Chem.* **1995**, *38*, 1267–1272.
(24) Haklai, R.; Gana-Weisz, G.; Elad, G.; Paz, A.; Marciano, D.; Egozi, Y.; Ben Baruch, G.; Kloog, Y. Dislodgment and accelerated degradation of Ras. *Biochemistry* **1998**, *37*, 1306–1314.
(25) Barkan, B.; Starinsky, S.; Friedman, E.; Stein, R.; Kloog, Y. The Ras inhibitor farnesylthiosalicylic acid as a potential therapy for neurofibromatosis type 1. *Clin. Cancer Res.* **2006**, *12*, 5533–5542.
(26) Blum, R.; Jacob-Hirsch, J.; Amariglio, N.; Rechavi, G.; Kloog, Y. Ras inhibition in glioblastoma down-regulates hypoxia-inducible factor-1alpha, causing glycolysis shutdown and cell death. *Cancer Res.* **2005**, *65*, 999–1006.
(27) Haklai, R.; Elad-Sfadia, G.; Egozi, Y.; Kloog, Y. Orally administered FTS (Salirasib) inhibits human pancreatic tumor growth in nude mice. *Cancer Chemother. Pharmacol.* **2007**, in press.
(28) Yaari, S.; Jacob-Hirsch, J.; Amariglio, N.; Haklai, R.; Rechavi, G.; Kloog, Y. Disruption of cooperation between Ras and MycN in human neuroblastoma cells promotes growth arrest. *Clin. Cancer Res.* **2005**, *11*, 4321–4330.
(29) Zundelevich, A.; Elad-Sfadia, G.; Haklai, R.; Kloog, Y. Suppression of lung cancer tumor growth in a nude mouse model by the Ras inhibitor Salirasib (farnesylthiosalicylic acid). *Mol. Cancer Ther.* **2007**, *31*, 31.
(30) Blum, R.; Elkon, R.; Yaari, S.; Zundelevich, A.; Jacob-Hirsch, J.; Rechavi, G.; Shamir, R.; Kloog, Y. Gene Expression Signature of Human Cancer Cell Lines Treated with the Ras Inhibitor Salirasib (*S*-Farnesylthiosalicylic Acid). *Cancer Res.* **2007**, *67*, 3320–3328.
(31) Blum, R.; Nakdimon, I.; Goldberg, L.; Elkon, R.; Shamir, R.; Rechavi, G.; Kloog, Y. E2F1 identified by promoter and biochemical analysis as a central target of glioblastoma cell-cycle arrest in response to Ras inhibition. *Int. J. Cancer* **2006**, *119*, 527–538.
(32) Aharonson, Z.; Gana-Weisz, M.; Varsano, T.; Haklai, R.; Marciano, D.; Kloog, Y. Stringent structural requirements for anti-Ras activity of S-prenyl analogues. *Biochim. Biophys. Acta* **1998**, *1406*, 40–50.
(33) Shohami, E.; Yatsiv, I.; Alexandrovich, A.; Haklai, R.; Elad-Sfadia, G.; Grossman, R.; Biegon, A.; Kloog, Y. The Ras inhibitor *S-trans*,*trans*-farnesylthiosalicylic acid exerts long-lasting neuroprotection in a mouse closed head injury model. *J. Cereb. Blood Flow Metab.* **2003**, *23*, 728–738.
(34) Weisz, B.; Giehl, K.; Gana-Weisz, M.; Egozi, Y.; Ben-Baruch, G.; Marciano, D.; Gierschik, P.; Kloog, Y. A new functional Ras antagonist inhibits human pancreatic tumor growth in nude mice. *Oncogene* **1999**, *18*, 2579–2588.
(35) Gana-Weisz, M.; Haklai, R.; Marciano, D.; Egozi, Y.; Ben Baruch, G.; Kloog, Y. The Ras antagonist *S*-farnesylthiosalicylic acid induces inhibition of MAPK activation. *Biochem. Biophys. Res. Commun.* **1997**, *239*, 900–904.
(36) Schroeder, H.; Leventis, R.; Rex, S.; Schelhaas, M.; Nagele, E.; Waldmann, H.; Silvius, J. R. *S*-Acylation and plasma membrane targeting of the farnesylated carboxyl-terminal peptide of *N*-ras in mammalian fibroblasts. *Biochemistry* **1997**, *36*, 13102–13109.
(37) Berrozpe, G.; Schaeffer, J.; Peinado, M. A.; Real, F. X.; Perucho, M. Comparative analysis of mutations in the p53 and K-ras genes in pancreatic cancer. *Int. J. Cancer* **1994**, *58*, 185–191.
(38) Guha, A.; Feldkamp, M. M.; Lau, N.; Boss, G.; Pawson, A. Proliferation of human malignant astrocytomas is dependent on Ras activation. *Oncogene* **1997**, *15*, 2755–2765.
(39) Chiu, V. K.; Silletti, J.; Dinsell, V.; Wiener, H.; Loukeris, K.; Ou, G.; Philips, M. R.; Pillinger, M. H. Carboxyl methylation of Ras regulates membrane targeting and effector engagement. *J. Biol. Chem.* **2004**, *279*, 7346–7352.
(40) Rando, R. R. Chemical biology of protein isoprenylation/methylation. *Biochim. Biophys. Acta* **1996**, *1300*, 5–16.
(41) Marom, M.; Haklai, R.; Ben Baruch, G.; Marciano, D.; Egozi, Y.; Kloog, Y. Selective inhibition of Ras-dependent cell growth by farnesylthiosalisylic acid. *J. Biol. Chem.* **1995**, *270*, 22263–22270.
(42) Ashery, U.; Yizhar, O.; Rotblat, B.; Elad-Sfadia, G.; Barkan, B.; Haklai, R.; Kloog, Y. Spatiotemporal Organization of Ras Signaling: Rasosomes and the Galectin Switch. *Cell. Mol. Neurobiol.* **2006**, *26*, 469–493.
(43) Hoffman, G. R.; Nassar, N.; Cerione, R. A. Structure of the Rho family GTP-binding protein Cdc42 in complex with the multifunctional regulator RhoGDI. *Cell* **2000**, *100*, 345–356.
(44) Scheffzek, K.; Stephan, I.; Jensen, O. N.; Illenberger, D.; Gierschik, P. The Rac-RhoGDI complex and the structural basis for the regulation of Rho proteins by RhoGDI. *Nat. Struct. Biol.* **2000**, *7*, 122–126.
(45) Mondal, M. S.; Wang, Z.; Seeds, A. M.; Rando, R. R. The specific binding of small molecule isoprenoids to rhoGDP dissociation inhibitor (rhoGDI). *Biochemistry* **2000**, *39*, 406–412.
(46) Michaelson, D.; Silletti, J.; Murphy, G.; D'Eustachio, P.; Rush, M.; Philips, M. R. Differential localization of Rho GTPases in live cells: regulation by hypervariable regions and RhoGDI binding. *J. Cell Biol.* **2001**, *152*, 111–126.
(47) Ding, J.; Lu, D. J.; Perez Sala, D.; Ma, Y. T.; Maddox, J. F.; Gilbert, B. A.; Badwey, J. A.; Rando, R. R. Farnesyl-L-cysteine analogs can inhibit or initiate superoxide release by human neutrophils. *J. Biol. Chem.* **1994**, *269*, 16837–16844.
(48) Tan, E. W.; Perez Sala, D.; Canada, F. J.; Rando, R. R. Identifying the recognition unit for G protein methylation. *J. Biol. Chem.* **1991**, *266*, 10719–10722.
(49) de Rooij, J.; Bos, J. L. Minimal Ras-binding domain of Raf1 can be used as an activation-specific probe for Ras. *Oncogene* **1997**, *14*, 623–625.

JM801165R